Geophysical Research Letters

Supporting Information for

Intensification and dynamics of the westward Equatorial Undercurrent during the summers of 1998 and 2016 in the Indian Ocean

Ke Huang,[1,2,3] Dongxiao Wang,[4*] Gengxin Chen,[1,3] Motoki Nagura,[5] Weiqing Han,[6] Michael J. McPhaden,[7] Ming Feng,[8] Ju Chen,[1*] Ying Wu,[9] Xiaolin Zhang,[10] Yuanlong Li,[11] Qiang Xie,[12†] Weiqiang Wang,[1,3] Feng Zhou,[2]

[1] State Key Laboratory of Tropical Oceanography, South China Sea Institute of Oceanology, Guangzhou, China

[2] State Key Laboratory of Satellite Ocean Environment Dynamics, Second Institute of Oceanography, Ministry of Natural Resources, Hangzhou, China

[3] Southern Marine Science and Engineering Guangdong Laboratory (Guangzhou), Guangzhou, China

[4] School of Marine Sciences, Sun Yat-sen University and Southern Marine Science and Engineering Guangdong Laboratory (Zhuhai), Zhuhai, China

[5] Japan Agency for Marine-Earth Science and Technology, Yokosuka, Japan

[6] Department of Atmospheric and Oceanic Sciences, University of Colorado, Boulder, Boulder, Colorado, USA

[7] Pacific Marine Environmental Laboratory, National Oceanic and Atmospheric Administration, Seattle, Washington, USA

[8] CSIRO Oceans and Atmosphere, Crawley, Western Australia, Australia

[9] State Key Laboratory of Estuarine and Coastal Research, East China Normal University, Shanghai, China

[10] Kyushu University, Fukuoka, Kyushu, Japan

[11] CAS Key Laboratory of Ocean Circulation and Waves, Institute of Oceanology, Chinese Academy of Sciences, Qingdao, China

[12] Institute of Deep-Sea Science and Engineering, Chinese Academy of Sciences, Sanya, China

†Deceased 26 June 2022

* Correspondence to: Dongxiao Wang, Ju Chen

Email: dxwang@scsio.ac.cn, jchen@scsio.ac.cn

Contents of this file:

1. Baroclinic Structure Function

The linear equations of motion including the wind forcing terms are:

$$u_t - f_0 v + \frac{1}{\bar{\rho}}\frac{\partial P}{\partial x} = \tau^x \mathbb{Z}(z) + (\nu u_z)_z + \nu_2 \nabla^2 u \quad (1)$$

$$v_t + f_0 u + \frac{1}{\bar{\rho}}\frac{\partial P}{\partial y} = \tau^y \mathbb{Z}(z) + (\nu v_z)_z + \nu_2 \nabla^2 v \quad (2)$$

$$\frac{\partial P}{\partial z} = -\rho g \quad (3)$$

$$\frac{\partial u}{\partial x} + \frac{\partial v}{\partial y} + \frac{\partial w}{\partial z} = 0 \quad (4)$$

$$\frac{\partial \rho}{\partial t} + w\frac{\partial \bar{\rho}}{\partial z} = 0 \quad (5)$$

where *u*, *v*, and *w* are the zonal, meridional and vertical velocity anomalies; *P* and ρ are the pressure and density anomalies, g is the acceleration due to gravity, $f = \beta y$ is the Coriolis parameter. The parameter ν is the coefficient of vertical eddy viscosity and ν_2 is the coefficient of Laplacian mixing. τ^x and τ^y are zonal and meridional wind-stress that forcing the ocean system, and wind-stress enters the ocean as body force with the vertical structure $\mathbb{Z}$(z).

Firstly, we consider the vertical mode decomposition and reduce the Eqs. (3) and (5) to:

$$\frac{1}{\bar{\rho}}\frac{\partial^2 P}{\partial t \partial z} = -N^2 w \quad (6)$$

$$N^2 = -\frac{g}{\bar{\rho}}\frac{\partial \bar{\rho}}{\partial z} \quad (7)$$

where *N* is the Brunt-Väisälä frequency, which is calculated from the vertical profile of potential density of the ORAS-5 and WOA18 data near the equator. Considering the shallow water approximation and vertically continuous stratification, horizontal velocity and pressure are then written as following:

$$(u, v, P) = \sum_{n=0}^{\infty} \big(u_n(x,y,t), v_n(x,y,t), p_n(x,y,t)\big)\, \psi_n(\mathrm{z}) \quad (8)$$

Using the continuity equation, we have

$$\frac{\partial w}{\partial z} = -\frac{\partial u}{\partial x} - \frac{\partial v}{\partial y} = -\sum\left(\frac{\partial u_n(x,y,t)}{\partial x} + \frac{\partial v_n(x,y,t)}{\partial y}\right)\psi_n(\mathrm{z}) = \sum_{n=0}^{\infty}\big(w_n(x,y,t)\big)\,\psi_n(\mathrm{z}) \quad (9)$$

Here, we assume $w_n(x,y,t) = -\frac{\partial u_n(x,y,t)}{\partial x} - \frac{\partial v_n(x,y,t)}{\partial y}$.

Vertically integrated the Eq. (9), we have

$$w = \sum_{n=0}^{\infty} \left(w_n(x,y,t)\right) S_n(\mathrm{z}), \quad [\frac{\partial S_n(\mathrm{z})}{\partial z} = \psi_n(\mathrm{z})] \tag{10}$$

where $S_n(\mathrm{z})$ is the vertical structure functions of vertical velocity. Substitution of the Eqs. (8) and (10) into Eq. (6) gives:

$$\sum_{n=0}^{\infty} \left(\frac{1}{\bar{\rho}} \frac{\partial^2 p_n(x,y,t)\psi_n(\mathrm{z})}{\partial t \partial z}\right) = -N^2 \sum_{n=0}^{\infty} \left(w_n(x,y,t)\right) S_n(\mathrm{z}) \tag{11}$$

$$\frac{d\psi_n(\mathrm{z})/\mathrm{dz}}{N^2 S_n(\mathrm{z})} = \frac{\bar{\rho} w_n}{\partial p_n/\partial t} = -\frac{1}{c_n^2} \tag{12}$$

As the first term in the Eq. (12) is a function of *z* alone and the second term is a function of (*x*, *y*, *t*) alone, for consistency both terms must be equal to a constant. Here we take the "separation constant" to be $-1/c_n^2$ as in (12), and the eigenvalue c_n is also known as the characteristic speed for the mode *n*. Then, the vertical structure is given as:

$$\frac{1}{N^2} \frac{d\psi_n(\mathrm{z})}{\mathrm{dz}} = -\frac{1}{c_n^2} S_n(\mathrm{z}) \tag{13}$$

Taking the *z*-derivative, we have

$$\frac{d}{\mathrm{dz}} \left(\frac{1}{N^2} \frac{d\psi_n(\mathrm{z})}{\mathrm{dz}}\right) + \frac{1}{c_n^2} \psi_n(\mathrm{z}) = 0 \tag{14}$$

This eigenvalue equation is solved under the condition $\int_{-H_{bot}}^{0} \psi_n dz = 0$, where H_{bot} is the bottom depth. The $\psi_n(\mathrm{z})$ form a set of orthogonal functions and are normalized by $\psi_n(0) = 1$ for all *n*. We solved this eigenvalue problem numerically obtaining N^2 from the vertical density profile of the ORAS-5. The $\psi_n(\mathrm{z})$ can be calculated by the MATLAB m-file obtained from https://github.com/sea-mat/dynmodes. The solutions of baroclinic structure functions for 1st–6th modes and their characteristic speeds are illustrated in Fig. S3 and Table S1.

2. Continuously Stratified Model and Damper Experiment

A continuously stratified LOM was used to assess the importance of the equatorial baroclinic waves for the intensification of westward EUC in the Indian Ocean. This model is described in detail in McCreary (1981), and has been applied to explain the dynamics of the East Indian Coastal Current, EUC, western boundary reflection, and basin resonances (Chen et al., 2015; Han et al., 2011; McCreary et al., 1996; Shankar et al., 1996; Yuan and Han, 2006). It has been demonstrated that the LOM is able to reasonably simulate the observed zonal current variability at the intraseasonal, seasonal, and interannual timescales in the TIO (e.g., Han, 2005; Han et al., 2011; Chen et al., 2015).

In the LOM, the equations of motion are linearized about a background state of rest with a realistic stratification represented by Brünt-Väisälä frequency, and the ocean bottom is assumed flat at 4000 m. With these restrictions, the solutions can be represented as expansions in the vertical normal modes (*n*) of the system. The zonal velocity *u*, meridional velocity *v* and pressure *p* in the solutions can be represented as expansions in the vertical normal modes of the system with eigenfunctions ψ_n(z):

$$u = \sum_{n=0}^{N} u_n \psi_n, \qquad (15)$$

$$v = \sum_{n=0}^{N} v_n \psi_n, \qquad (16)$$

$$p = \sum_{n=0}^{N} p_n \psi_n, \qquad (17)$$

where the expansion coefficients, u_n, v_n and p_n are functions only of *x*, *y*, and *t*. Strictly speaking, the total mode number should extend to infinity, but the solutions converge rapidly enough with *n* (McCreary et al., 1996; Shankar et al., 1996). Herein *n* = 25 is selected to represent the total baroclinic mode number (same as in Han et al., 2011; Chen et al., 2015). The total solution is the sum of all the selected modes. The terms u_n, v_n and p_n are governed by the follow equations:

$$\left(\partial_t + \frac{A}{c_n^2}\right)u_n - fv_n + \frac{1}{\bar{\rho}} p_{nx} = \tau^x Z_n / \left(\bar{\rho} H_n\right) + v_h \nabla^2 u_n - \delta u_n, \qquad (18)$$

$$\left(\partial_t + \frac{A}{c_n^2}\right)v_n + fu_n + \frac{1}{\bar{\rho}} p_{ny} = \tau^y Z_n / \left(\bar{\rho} H_n\right) + v_h \nabla^2 v_n, \qquad (19)$$

$$\left(\partial_t + \frac{A}{c_n^2}\right)\frac{p_n}{\bar{\rho}c_n^2} + u_{nx} + v_{ny} = 0 \qquad (20)$$

,

where c_n is the characteristic speed of equatorial Kelvin wave for vertical mode number n. The c_n values for the first six baroclinic modes (n = 1,2, …, 6), estimated from a mean background stratification based on density observations in the Indian Ocean (see Moore and McCreary, 1990), are 264, 167, 105, 75, 60 and 49 cm s^{-1}. The Coriolis parameter is $f = \beta y$ under equatorial β–plane approximation and v_h is the coefficient of the horizontal eddy viscosity. The coupling intensity of each mode to the wind field is determined by $Z_n = \int_{-D}^{0} Z(z)\, \psi_n dz/H_n$, $H_n = \int_{-D}^{0} \psi_n^2 dz$, and $Z(z)$ is the vertical profiles of wind that is introduced as a body force, where $Z(z)$ is constant in the upper 50 m and linearly decreases to zero from 50 to 100 m depth. The terms associated with A/c_n^2 represent vertical friction with A = 0.00013 cm^2 s^{-3}, and they provide damping for the equatorial Kelvin and Rossby waves. Since the damping is inversely proportional to c_n^2, the low order baroclinic modes Kelvin and Rossby waves experience weak damping effects because of their faster speeds (e.g., $c_1 = 264$ cm s^{-1} and $c_2 = 167$ cm s^{-1}), and thus they can propagate far away from the forcing region. By contrast, the higher order modes experience strong damping effects due to their slower speeds, and thus their response is local and manly restricted to the forcing region (see Han, 2005 for detailed discussions). All solutions of the control run have a damper with coefficient $\delta(x, y)$ near the eastern boundary of the basin (in the last term of the Eq. 2a), as discussed next, to absorb the energy of forced equatorial Kelvin wave in this region.

The LOM with a realistic Indian Ocean basin without the Maldives Islands was first spun up for 20 years forced with monthly mean climatology of cross-calibrated, multi-platform version 2 (CCMP v2), for the 1988–2016 period. Restarting from the spin up run, the LOM was integrated forward in time using monthly CCMP winds from 1988 to 2016. This solution is referred to as the LOM main run (LOM-MR) and the total solution of LOM-MR is the sum of the first 25 modes. Then, a second run was performed with a damper in the eastern equatorial ocean to isolate the effects of eastern boundary reflected Rossby waves. This damper with coefficient $\delta(x,y)$ (Eq. 18) is nonzero only in the eastern equatorial ocean within the region x > 97.5°E, –7.5°S < y < 7.5°N. In this region, δ has a maximum value of $0.6c_n/\Delta x$, where Δx is the zonal grid step, and δ decreases linearly to zero within 5° of its western edge and within 2° of its northern and southern edges. This damper causes equatorial Kelvin waves to decay rapidly in an e-folding scale of ~1.5 Δx.Therefore, the damper efficiently absorbs the energy of incoming equatorial Kelvin waves, and thus no Rossby waves are reflected back into the ocean interior from the eastern boundary (e.g., McCreary et al., 1981, 1996; Han et al., 2005, 2011). We refer to this run as LOM-DAMP. The difference between the two experiments (LOM-MR minus LOM-DAMP, defined as LOM-Reflect) linearly isolates the reflected Rossby wave effects.

3. Forced and Reflected Intermediate-order Baroclinic Mode Waves

Here, we elucidate the contributions of different baroclinic modes to subsurface zonal velocity anomalies. For the LOM, the velocity anomalies for each baroclinic mode were obtained from the model results. For the comparison between the LOM and ORAS-5, the decomposition from each baroclinic mode was further obtained from ORAS-5. The decomposition of ORAS-5 is performed with the climatological density profile averaged over the near-equatorial region (2.5°S to 2.5°N) and then by projecting zonal velocities onto the vertical profiles of the first 8 baroclinic modes.

In our model, three parameters affect the relative amplitudes of the baroclinic modes. The first is the propagation speed of waves (c_n), the second is the coupling efficiency (P_n) with which the wind forcing projects onto the baroclinic mode structures and the third is the vertical positions of the modal zero crossings, as well as the modal peaks and troughs (Fig. S3). The coupling efficiency is defined as $P_n = \frac{\frac{1}{h_{mix}}\int_{-h_{mix}}^{0}\psi_n(z)dz}{\int_{-H_{bot}}^{0}\psi_n^2(z)dz}$, where h_{mix} = 60 m is the mean mixed layer depth and H_{bot} = 4000 m is the ocean floor depth. A baroclinic mode is excited efficiently by winds if this parameter is large. According to this parameter, the first and second baroclinic modes are most favorably excited (see Table S1). However, waves of these modes propagate so fast (c_1 = 264 cm

s^{-1}, c_2 = 167 cm s^{-1}, Table S1) that zonal velocity anomalies due to reflected waves are opposite in direction to those of directly forced waves during 1997–1998 and 2015–2016, which results in the destructive interference at the central basin. In contrast, intermediate-order (mainly 3rd to 6th) baroclinic mode waves propagate much slower, and zonal velocity anomalies due to forced waves reverse their sign when reflected waves reach the central basin (Figs. S4 E–H). The large amplitudes of the 3rd to 6th baroclinic modes in Fig. 4G are due to this constructive relationship between forced and reflected waves, which builds unique and strong flow in the depth range of 100–200 m. The amplitude of the 4th baroclinic mode is largest, which is because P_n for this mode is larger than those for other intermediate modes and that the vertical structure of this mode has a sharp trough at about 100 to 200 m depths (Table S1 and Fig. S3). The vertical profile of the *n*th baroclinic mode has *n* zero crossings, and other intermediate modes suffer from the relatively small amplitude of vertical structure function and visible phase jump with their first zero crossing near 100–200 m depths (Table S1 and Fig. S3).

4. **Equatorial moored observation and model validation**

The equatorial in-situ observations derived from the ADCPs (velocity, Fig. S2) and SBE 37-SM (temperature, Fig. S2) are also used to validate the ORAS-5 results. The ADCPs mounted on subsurface moorings as part of the Research Moored Array for African–Asian–Australian Monsoon Analysis and Prediction (RAMA) (McPhaden et al., 2009) and SCSIO TIOON Q5 (Zeng et al., 2021). The observed subsurface zonal velocity are well captured by the ORAS-5, with similar spatial patterns and magnitudes (Fig. S1A). Note that the wEUC during JJ 2016 observed by the TIOON Q5 is missed due to the lack of buoyancy with the sinking mooring (Fig. S1B). Consistent with published information, the observed temperature in the depth range of 300–500 m are well simulated in the ORAS-5 reanalysis data (correlation coefficient with in-situ observations is about 0.95, 99% confidence level) (Fig. S2), showing the skill of the ORAS-5 in simulating the key dynamics of the equatorial subsurface zonal flows and thermal structures.

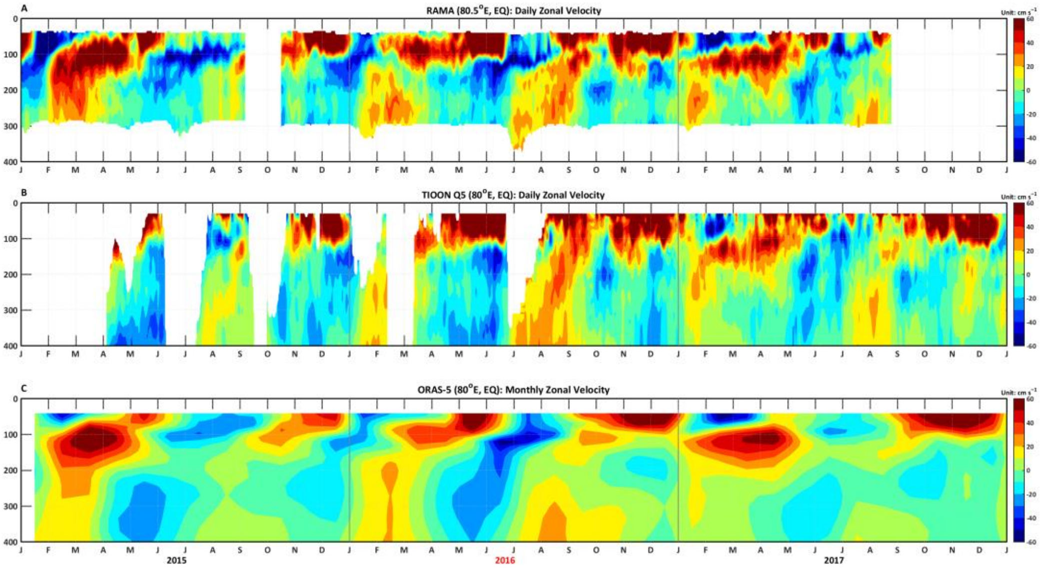

Figure S1. (**A**) Daily zonal velocity obtained from the RAMA mooring at (80.5°E, EQ) from 2015 to 2017. (**B**) As is in (A) but for the SCSIO TIOON mooring Q5 at (80°E, EQ). (**C**) Monthly zonal velocity at (80°E, EQ) obtained from the ORAS-5.

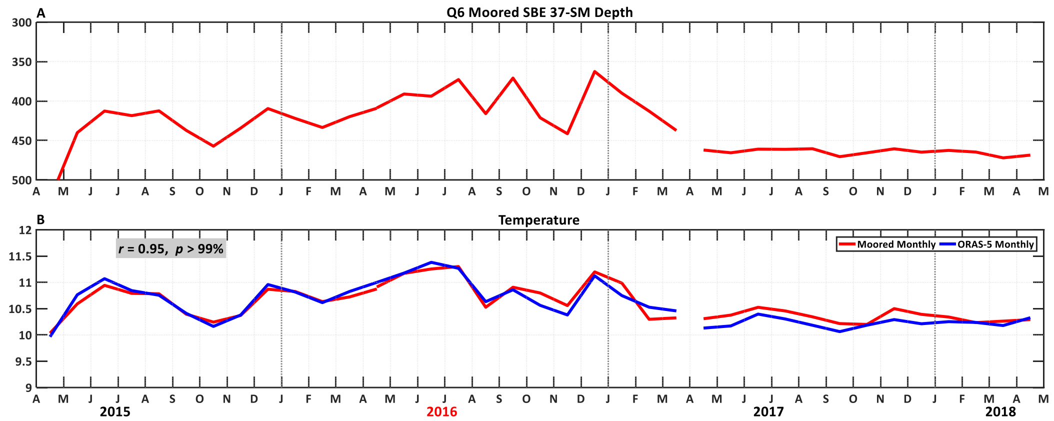

Figure S2. (**A**) Depth of SBE 37-SM (MicroCAT Conductivity and Temperature Recorder) mounted on the mooring Q6. (**B**) Temperature obtained from the moored SBE 37-SM (red line) and the ORAS-5 (blue line). The temperature obtained from ORAS-5 is interpolated onto the depth of SBE 37-SM.

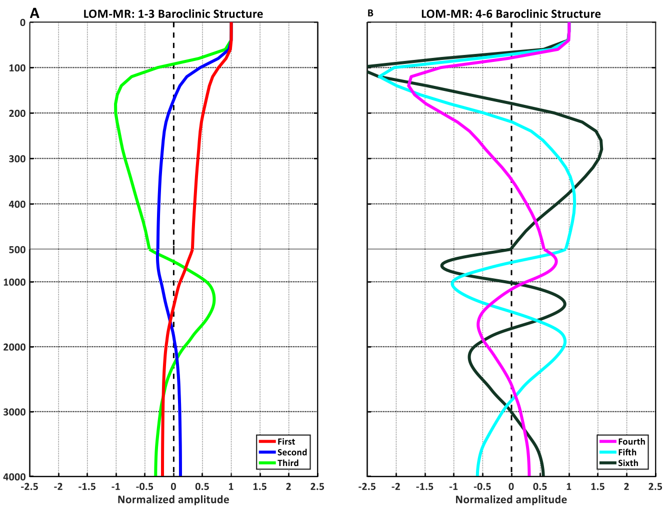

Figure S3. (**A**) Normalized vertical structure function of the first, second and third baroclinic modes derived from the mean Brunt-Väisälä frequency profiles obtained from tropical Indian Ocean observations (used in LOM). (**B**) Normalized vertical structure function of the fourth, fifth and sixth baroclinic modes used in LOM.

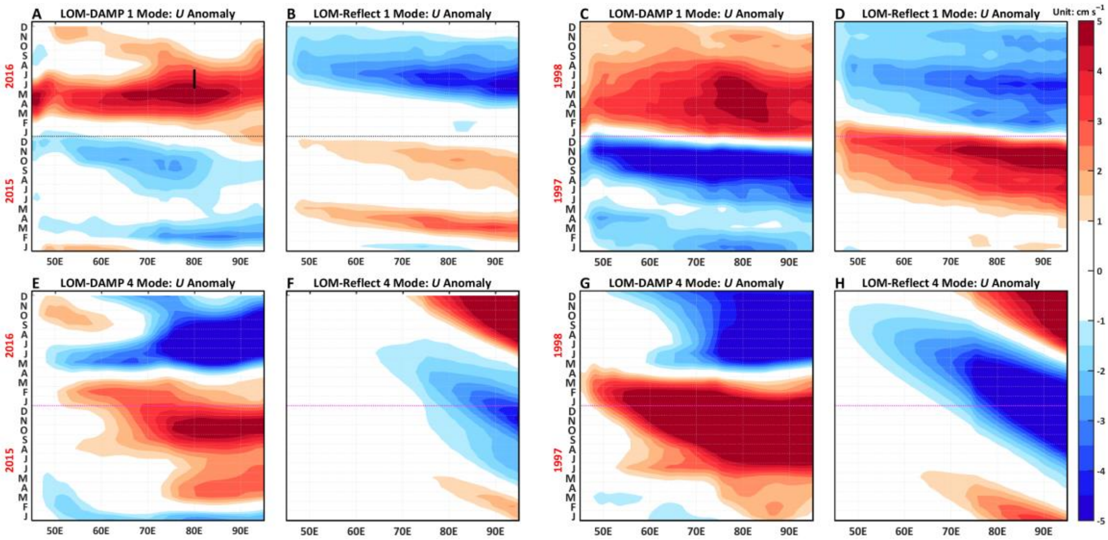

Figure S4. Zonal velocity anomalies of the first baroclinic mode averaged over 100-200 m depths and 2.5°S to 2.5°N obtained from (**A**) LOM-DAMP and (**B**) LOM-Reflect during 2015 and 2016. The black line is illustrated in panel (A) in JJ 2016 and at 80°E. (**C**, **D**) Same as panel (**A**, **B**), respectively, but for the period from 1997 to 1998. (**E**–**H**) Same as panels (A–D), respectively, but for the fourth baroclinic mode.

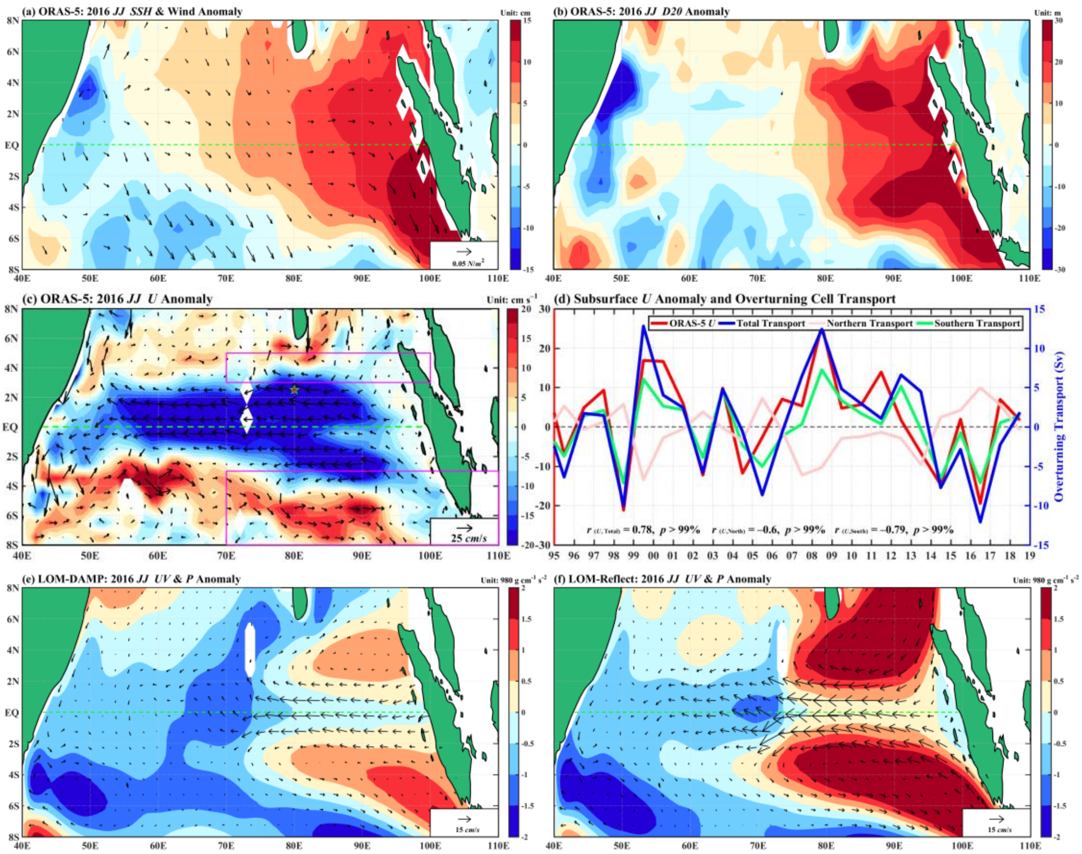

Figure S5. Spatial structures of 2016 JJ means of (**a**) sea surface height (SSH, colored shading) and wind stress (arrows), (**b**) thermocline depth (D20), (**c**) subsurface current vectors (arrows) and zonal velocity (colored shading) averaged between 100 and 200 m obtained from the ORAS-5. (**d**) The inter-annual variability of JJ mean equatorial undercurrent (red line) compared to anomalous subsurface transport of shallow overturning cell (blue line) (transport in the Southern Hemisphere minus transport in the Northern Hemisphere). The green and pink lines are anomalous subsurface transports of southern and northern shallow overturning cells as pink boxes in (c). (**e**) Current vectors (arrows) and pressure (colored shading) averaged between 100 and 200 m obtained from LOM-DAMP, and (**f**) current vectors (arrows) and pressure (colored shading) averaged over 100 to 200 m obtained from LOM-Reflect.

Table S1. Characteristics of the baroclinic modal decomposition using mean Brunt-Väisälä frequency profiles (0–4000 m) obtained from tropical Indian Ocean observations (Han et al., 2011). Results were almost the same as that of the mean Brunt-Vaisala frequency obtained from the ORAS-5. +/– represent the eastward/westward phase propagation.

Mode number	Characterisitc phase speed c_n (cm s^{-1})	Kelvin wave's phase speed ($\frac{\omega}{k}$, cm s^{-1})	1st meridional Rossby waves' phase speed ($\frac{\omega}{k}$, cm s^{-1})	Depth of first zero-crossing (m)	Depth of second zero-crossing (m)	Wind coupling efficiency (P_n, m^{-1})
1	264	+264	–88	1376	–	0.0036
2	167	+167	–56	171	1840	0.0058
3	105	+105	–35	92	690	0.0012
4	75	+75	–25	78.5	346	0.0011
5	60	+60	–20	70	219	0.0005
6	49	+49	–16	66	179	0.0005